Vibrational and Electronic Absorption Spectroscopy of 2,3-Benzofluorene and Its Cation

John Banisaukas, Jan Szczepanski, and Martin Vala*

Department of Chemistry and Center for Chemical Physics, University of Florida, Gainesville, Florida 32611-7200

So Hirata

William R. Wiley Environmental Molecular Sciences Laboratory, Pacific Northwest National Laboratory, P.O. Box 999, Richland, Washington 99352

Received: October 14, 2003

Benzofluorene ($C_{17}H_{12}$) has been studied in argon matrices via Fourier transform infrared and UV−visible absorption spectroscopy. The analysis of the infrared absorption spectra of neutral and cationic 2,3-benzofluorene was supported by density functional theory (DFT) B3LYP/6-311+G** calculations of the harmonic-mode frequencies. Extensive time-dependent DFT calculations of the electronic vertical excitation energies with BLYP/6-31++G** and B3LYP/6-31++G** functionals/basis sets and the Casida−Salahub asymptotic correction were performed to assign the observed electronic absorption bands of the neutral species. Although the observed low-energy absorption bands are predicted well by theory, the higher-energy bands ($S_n \leftarrow S_0$ transitions, $n \geq 4$) have been assigned only tentatively. However, the observed electronic absorption bands for the parent, singly dehydrogenated cationic and neutral species are in accord with TDDFT (BLYP/6-31G**) results. The possibility that the 2,3-benzofluorene cation contributes to the unidentified infrared (UIR) bands observed from interstellar space is discussed briefly.

I. Introduction

Polycyclic aromatic hydrocarbons (PAHs) in neutral, ionized, fragmented, and/or hydrogenated forms are widely considered to be the carriers of the unidentified infrared (UIR) emission bands.[1−4] Bands at 3.3, 6.2, 7.8, 8.6, and 11.3 μm have been observed in many carbon- and hydrogen-rich galactic and extragalactic regions near UV−visible sources. After a PAH molecule absorbs UV or visible radiation, the energy is distributed among highly excited vibrational modes in the ground electronic state. Deactivation occurs via infrared (IR) emission from the various PAH vibrational modes. Although the frequencies of these modes generally match the observed UIR bands, a specific set of PAHs has yet to be identified as the origin of the UIR bands.

Laboratory absorption spectra of PAH cations more closely mimic the intensity patterns of the UIR bands than do the spectra of PAH neutrals.[5−8] The variation of UIR intensity with distance from interstellar radiation sources supports the concept of a mixture of neutral and ionic PAHs as the carriers of the UIR bands.[9−12] Infrared photodissociation spectra of gas-phase PAH cations have been recently reported.[13−15] Mass-selected PAH cations stored in an ion trap were dissociated by multiphoton absorption during irradiation with the tunable output of a free-electron laser. To determine the effect of vibrational energy on the IR emission process, Saykally and co-workers recently studied several vapor-phase neutral PAHs[16−18] and the pyrene cation[18] via single-photon IR emission spectroscopy. Increasing internal energy was found to broaden and red shift the emission bands. Although the PAHs studied did not reproduce the UIR bands, it was surmised that large PAHs were good candidates for the UIR carriers.[19] In addition, photofragmentation studies of PAHs, reported recently, contribute to our understanding of the photochemistry of the interstellar medium.[20−24]

The present paper focuses on the vibrational and electronic absorption spectroscopy of 2,3-benzofluorene (BZF) and its cation. In the following paper,[47] the photodissociation pathways of the 2,3-benzofluorene cation are described.

II. Computational Methods

Optimized geometries, fragmentation energies, and harmonic vibrational frequencies were calculated using the Gaussian 98 platform.[25] The B3LYP hybrid functional was applied in conjunction with the 6-31G** (or 6-311+G**) basis set. The larger 6-311+G** basis set generally yields more-accurate frequencies and intensities.[26,27]

The vertical excitation energies and oscillator strengths of neutral BZF and its cation and dehydrogenated neutral BZF and its cation were computed by the TDDFT method using the Becke−Lee−Yang−Parr (BLYP) functional at the respective B3LYP/6-31G** optimized geometries. The 6-31G** basis set was used for the excited-state calculation of the cations, and the 6-31++G** basis set was used for the neutral species. It has been shown that the TDDFT method with the BLYP/6-31G** functional and basis set reproduces the experimental vertical excitation energies of various PAH cations,[28] including PAH species related to fluorene,[29] with an average error of 0.3 eV and qualitatively correct intensity profiles. A similar degree of agreement between theory and experiment has been observed for PAH anions by using the same functional and the 6-31++G** basis set.[28]

TDDFT, employing many of the widely used exchange-correlation functionals (including the BLYP), is known to

* To whom correspondence should be addressed. E-mail: mvala@chem.ufl.edu.

10.1021/jp031163n CCC: $27.50
Published on Web 04/02/2004

underestimate excitation energies to high-lying excited states substantially.[30,31] To assess and rectify this problem, calculations were also performed with the BLYP and B3LYP functionals and the 6-31++G** basis set and the Casida−Salahub asymptotic correction[30,32] for neutral species, where this problem is expected to be more severe than in the cation species. In this method, a $-1/r$ asymptotic tail was spliced to the valence region of the BLYP or B3LYP exchange-correlation potential, which was decreased by a constant factor to ensure a seamless transition between the two curves. The constant factor, which amounts to the difference between the true ionization potential and that estimated by Koopmans' approximation, was determined either by a separate ΔSCF-type calculation that provided the ionization potential of the neutral species or by the phenomenological linear relationship between the highest occupied KS orbital energies and the ionization potentials.[33] The excitation-energy calculations were performed by using massively parallel DFT and TDDFT implementations[33] of the NWChem quantum chemistry program suite.[34]

III. Experimental Methods

Infrared and electronic absorption spectra were collected for neutral BZF and its radical cation isolated in argon matrices at 12 K. The experimental apparatus is similar to that used in earlier PAH studies.[29,35,36] Briefly, the deposition surface was either a BaF_2 or CsI window cooled to 12 K by a closed-cycle helium cryostat (Displex HC-2, APD Cryogenics Inc.). Neutral BZF spectra were collected after co-depositing BZF vapor with argon (99.995% purity, Matheson) on a CsI window. Solid BZF was vaporized in a quartz oven heated to ∼40 °C. During deposition (2−4 h), the concentration ratio of argon atoms to BZF molecules was approximately 300:1. After deposition, the infrared absorption spectrum (4000−700 cm^{-1}) was collected at 1 cm^{-1} resolution using a MIDAC M2000 FT-IR spectrometer. The electronic absorption spectrum (800−200 nm) was collected on the same matrix at a bandwidth of 0.28 nm with an IBM 9420 UV−visible spectrophotometer.

For BZF cations, carbon tetrachloride (Kodak, Spectrograde) was added to the argon gas to enhance the ionization yield.[37] The gas mixture (99.7% Ar, 0.3% CCl_4) was electron bombarded with a homemade electron gun located ca. 3 cm from the deposition window. The electrons were accelerated toward the deposition region by a +90 V potential applied to a ring electrode located 5 mm in front of the deposition window. Electron current (typically ca. 30−50 μA) was monitored on a microammeter in line with the ring electrode. The predominant BZF ionization mechanisms expected are Penning and charge-transfer ionization because Ar atoms were ca. 300 times more abundant than BZF in the ionization region. Argon atoms excited by low-energy electrons collide with and ionize BZF neutral molecules (IE = 7 eV). Because matrix charge neutrality is crucial to cation accumulation in the matrix, chlorine anions are added by electron bombardment of CCl_4.

Vibrational and electronic bands were correlated by annealing the matrix to 34 K and by photolyzing the matrix with UV−visible light (225−900 nm, 100-W medium-pressure Hg lamp). During annealing, electrons are free to move throughout the matrix, resulting in the neutralization of trapped cations. Similarly, electrons liberated from trapped anions during UV irradiation are captured by the BZF cations, resulting in cation neutralization. Ultraviolet irradiation can also photofragment trapped species. After annealing and/or photolysis, infrared and UV−visible spectra were re-collected for comparison with spectra from the original, unaltered matrix.

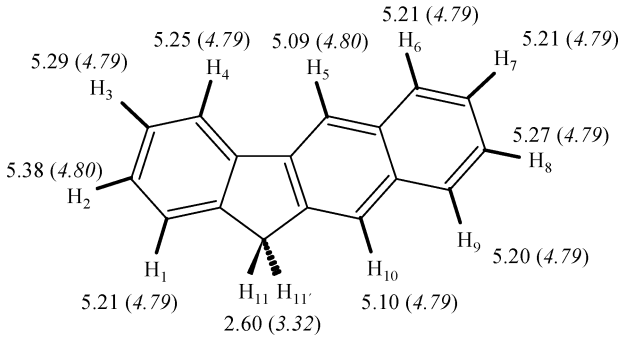

Figure 1. Structure of 2,3-benzofluorene. Values shown are C−H bond energies (eV) for the cation (*neutral*) calculated at the B3LYP/6-31G** level of theory.

IV. Results and Discussion

A. Infrared Absorption Spectra. *1. Neutral BZF.* The observed infrared absorption spectrum of neutral BZF is compared to calculated harmonic frequencies in Figure 2. To account for mode anharmonicities, the B3LYP/6-311+G** and B3LYP/6-31G** frequencies were scaled by factors of 0.98 and 0.97, respectively. Frequencies calculated with the 6-311+G** basis set provided a slightly better fit to the experimental bands. Band frequencies, relative intensities, and mode descriptions for the observed (solid Ar) and calculated (6-311+G**) spectra are listed in Table 1. Substructure was observed on all experimental bands because of the isolation of BZF in different matrix sites. Only the most intense subband is listed. Tabulated experimental band intensities were determined by summing the subband intensities.

All observed bands were assignable to calculated frequencies. Differences between observed and calculated frequencies in the 400−1700 cm^{-1} region were less than 12 cm^{-1}. However, large shifts (30−60 cm^{-1}) were observed for the C−H stretching modes in the 2900−3200 cm^{-1} range. The average experimental Ar matrix-gas-phase frequency shifts in the CH stretching region, for the five PAHs studied in ref 38, are small, less than 3 cm^{-1}. Therefore, the 30−60 cm^{-1} frequency shifts observed are not likely to be due to the matrix environment but are mainly due to the larger CH stretching mode anharmonicities. Thus, large energy shifts reflect the inability of a single scaling factor to account for anharmonicities associated with different vibrational mode types. Tabulated experimental band intensities are relative to the intensity of the 771.5 cm^{-1} band. Calculated intensities are relative to the 769.6 cm^{-1} band (41.9 km/mol). As expected for neutral PAH molecules, the C−H out-of-plane bending modes in the 700−1000 cm^{-1} range were stronger than the C−C stretches and C−H in-plane bends in the 1000−1650 cm^{-1} region. Small energy differences between calculated and experimental band positions in the IR spectra of the BZF neutral demonstrate that the B3LYP functional is reliable in predicting vibrational (and structural) properties of BZF.

2. BZF Cation. Infrared absorption spectra, collected after electron bombardment of the gas mixture, are shown in Figures 3 and 4. The lower spectrum is the IR spectrum of neutral BZF, shown previously. The middle spectrum corresponds to the electron-bombarded gas mixture. The upper spectrum was recorded after annealing (to 34 K) the matrix containing the electron bombardment products. Bands corresponding to CCl_3, CCl_3^+, and the CCl_3·Cl complex were assigned on the basis of previous studies.[37] Warming the matrix to 34 K reduced several bands by 20−30%. Bands previously assigned to the BZF neutral remained essentially unchanged. The bands reduced upon annealing were assigned to BZF cations trapped in the matrix.

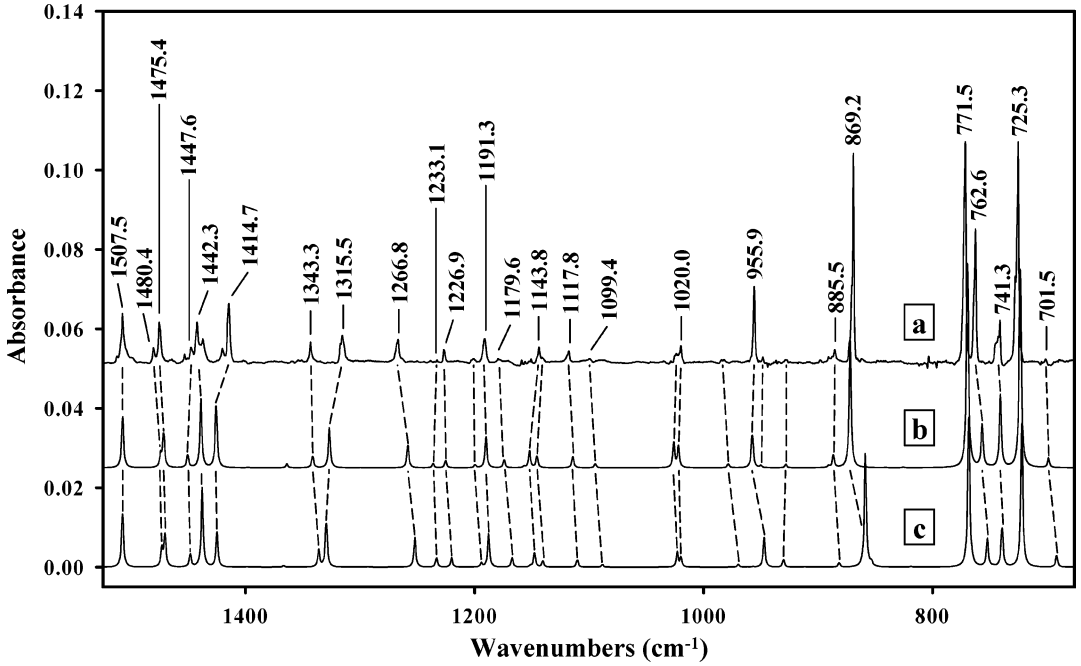

Figure 2. Experimental and calculated infrared absorption spectra (1525−675 cm^{-1}) for neutral 2,3-benzofluorene ($C_{17}H_{12}$). (a) IR absorption spectrum of 2,3-benzofluorene isolated in solid Ar at 12 K. (b) IR absorption spectrum calculated at the B3LYP/6-311+G** level of theory (scaled by 0.98). (c) IR absorption spectrum calculated at the B3LYP/6-31G** level of theory (scaled by 0.97).

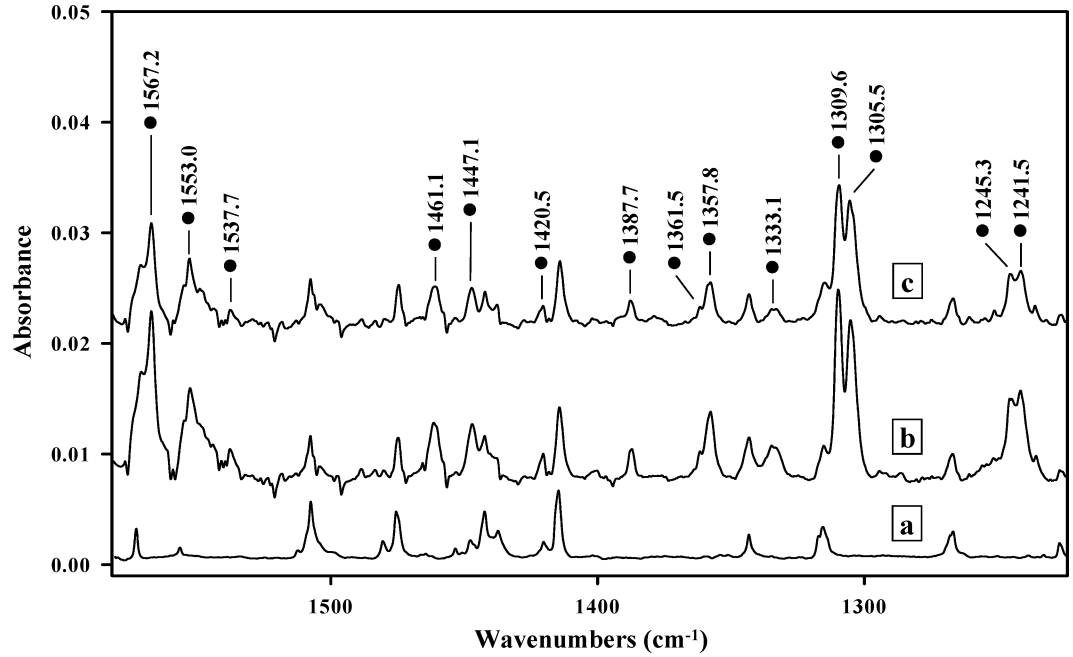

Figure 3. Experimental infrared absorption spectra (1580−1225 cm^{-1}) of neutral and cationic 2,3-benzofluorene isolated in solid Ar at 12 K. Bands assigned to the 2,3-benzofluorene cation are labeled with black dots. (a) IR absorption spectrum of neutral 2,3-benzofluorene. (b) IR absorption spectrum of neutral and cationic 2,3-benzofluorene with 0.1% CCl_4 added to Ar. (c) IR absorption spectrum recorded after annealing matrix b to 34 K.

Vibrational frequencies for the BZF cation were calculated at the B3LYP/6-311+G** level of theory with a scaling factor of 0.98. Frequencies and relative intensities are listed in Table 2. The integral intensity of the calculated 1571.6 cm^{-1} band is 359.3 km/mol. As expected for PAH cations, the C−C stretches and C−H in-plane bends in the 1000−1650 cm^{-1} region were stronger than the C−H out-of-plane bending modes in the 700−1000 cm^{-1} range. Several regions of the observed spectrum were inaccessible because of overlapping by other species. The spectral region from 880 to 940 cm^{-1} was dominated by the CCl_3 and CCl_3·Cl bands. The strong CCl_3^+ and CCl_3·Cl bands at 1036.3 and 1019.5 cm^{-1} prevented the observation of the cation band predicted at 1012.7 cm^{-1}. The 1580−1600 cm^{-1} spectral region was obscured by bands of H_2O trapped in the matrix. To display the correlation between calculated and observed cation frequencies better, a synthetic experimental spectrum was created on the basis of the observed cation bands (Figure 5). Synthetic bands with 3 cm^{-1} bandwidths were constructed for each observed cation frequency using 50% Gaussian and 50% Lorentzian functions. Intensities were assigned on the basis of the relative intensities observed in the matrix. Unlike the situation for some PAHs containing cyclo-

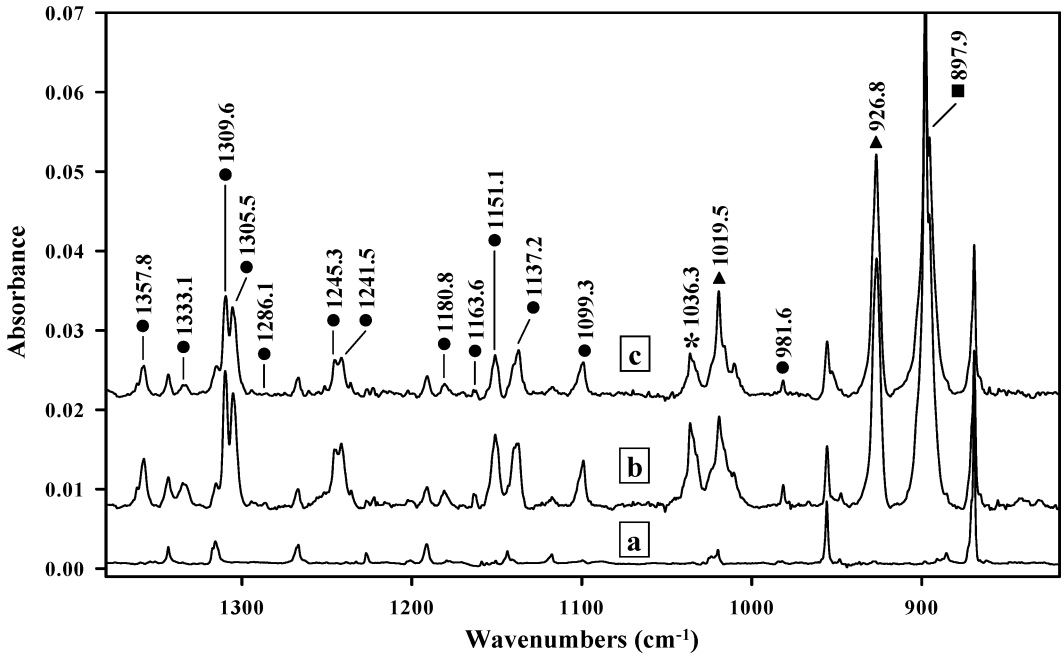

Figure 4. Experimental infrared absorption spectra (1380−820 cm^{-1}) of neutral and cationic 2,3-benzofluorene isolated in solid Ar at 12 K. Dots indicate 2,3-benzofluorene cation bands. Asterisks, triangles, and squares indicate bands due to CCl_3^+, CCl_3·Cl, and CCl_3, respectively. (a) IR absorption spectrum of neutral 2,3-benzofluorene. (b) IR absorption spectrum of neutral and cationic 2,3-benzofluorene with 0.1% CCl_4 added to Ar. (c) IR absorption spectrum recorded after annealing matrix b to 34 K.

pentadienyl ring,[36,39,40] overall good agreement was found here for the observed and predicted frequencies and relative intensities of the BZF cation.

B. Electronic Absorption Spectra. *1. Neutral BZF.* The electronic absorption spectrum of neutral BZF is presented in Figure 6. Transitions were assigned by comparing observed absorption bands to vertical excitation energies and oscillator strengths (*f*) calculated via TDDFT with the BLYP/6-31++G** functional/basis set (with and without the asymptotic correction) and the B3LYP/6-31++G** (with asymptotic correction) functional/basis set (Table 3). The observed bands at 337.3 nm (3.68 eV), 312.2 nm (3.97 eV), and 298.5 nm (4.15 eV) match calculated (BLYP) excitation energies within 0.3 eV and are thus assigned to transitions from the ground state to the first three excited electronic states. The relatively strong 282.0 nm band is separated by 1980 cm^{-1} from the adjacent lower-energy 0−0 transition. Therefore, it cannot be associated with a fundamental vibration in the S_3 state and must be assigned to the $S_4 \leftarrow S_0$ (0−0) transition.

The strongest observed band at 259.4 nm (4.78 eV) was assigned to the $S_5 \leftarrow S_0$ (0−0) transition on the basis of its relatively large predicted oscillator strength (0.5−0.7), close to the estimated experimental value of 1.1. The 333.3, 329.3, 326.4, 322.2, 321.5, and 315.1 nm vibronic bands (not marked in Figure 6, except for the 322.2 nm band) associated with the 337.3 nm band ($S_1 \leftarrow S_0$ (0−0) transition) are spaced 355, 719, 988, 1387, 1454, 1718, and 2086 cm^{-1}, respectively, from the 337.3 nm band. Assuming that the geometry for BZF is not greatly changed after electronic excitation, most of the above intervals can be described by ground-state vibrational modes. In fact, the calculated (B3LYP/6-311+G**, 0.98 scaled) Raman-active mode frequencies in the ground state of 350 (ring stretch, in-plane), 750 (C_5-C_{10} breathing), 974 ((CH_1, CH_3) and (CH_2, CH_4) out-of-plane, π phase), 1397 ((C_6-C_7 and C_8-C_9 stretch) + (C−H_6 and C−H_9 in-plane bend)), and 1450 cm^{-1} (CC stretch and CH in-plane bend) match quite well with the observed intervals in the S_1 state. The two remaining intervals may be assigned as combination modes: 1718 cm^{-1} = 719 + 988 cm^{-1} and 2086 cm^{-1} = 719 + 1387 cm^{-1}. Similarly, the 250.3 nm vibronic band of $S_5 \leftarrow S_0$ (Figure 6), spaced 1401 cm^{-1} from the 259.4 nm (0−0) band, can be described by the calculated 1397 cm^{-1} S_0 Raman-active mode.

In Table 3, the vertical excitation energies, calculated using the Casida−Salahub asymptotic correction, are given. A comparison of the calculated results with (and without) the asymptotic correction indicates their insensitivity to the correction, despite the fact that, in the asymptotic correction calculation, a large negative shift of ca. 2 eV has been added to the exchange-correlation potential in the valence region. This means that as many as 12 of the lowest-lying excited states of neutral BZF can be characterized as valence excited states. This is consistent with our previous findings that the BLYP functional without any asymptotic correction can describe the lowest excited states of anions reasonably accurately[28] because they are also valence excited states. However, this rules out the wrong asymptotic behavior of the exchange-correlation potential as the source of the relatively large deviations between theory and experiment for the $S_4 \leftarrow S_0$ and higher transitions. Rather, in view of the great sensitivity of the calculation results on exchange-correlation functionals, this may imply an alternative assignment in which weak absorption features between 260 and 300 nm are the fundamental transitions, although such an assignment does not seem to be in line with the calculated oscillator strengths. The assignments of $S_4 \leftarrow S_0$ and higher transitions, given in the table, are based on calculated intensities and excitation energies but should be viewed as tentative.

Because the infrared and electronic absorption spectra were recorded on the same matrix, the BZF concentration (*c*) and path length (*l*) are identical for each IR and UV−visible absorption. Thus, the molar absorptivity, ϵ_{UV}, for a UV band can be calculated on the basis of the relative IR and UV−visible band absorbances (*A*) from $\epsilon_{UV} = (A_{UV}/A_{IR})\epsilon_{IR}$. For the well-isolated observed band at 869.2 cm^{-1}, the closest calculated frequency is 872.0 cm^{-1}, which has a predicted integral intensity of 27 km/mol. Equating this value with $2.303\epsilon_{IR}\Delta\nu_{1/2}$ and adopting a $\Delta\nu_{1/2}$ bandwidth for the 869.2 cm^{-1} band of 2.2 cm^{-1},

TABLE 1: Comparison of the Calculated (B3LYP/6-311+G) and Experimental (Ar Matrix, 12 K) Infrared Absorption Spectrum of Neutral 2,3-Benzofluorene[a]**

mode description[b]	calcd (B3LYP/6-311+G**)[c,d]	exptl (Ar matrix)[e]
τ(CCC)	203.1 (0.05)	
τ(CCC)	267.8 (0.07)	
τ(CCC)	305.0 (0.02)	
τ(CCC)	396.0 (0.07)	
τ(CCC)	426.3 (0.04)	
τ(CCC)	472.5 (0.33)	474.2 (0.30)
α(CCC)	538.1 (0.02)	
α(CCC)	570.4 (0.18)	571.4 (0.17)
α(CCC)	605.2 (0.06)	605.7 (0.04)
τ(CCC)	663.8 (0.02)	663.7 (0.03)
α(CCC)	698.8 (0.05)	701.5 (0.03)
ϵ(CCH) + τ(CCC)	723.5 (0.93)	725.3 (1.00)
ϵ(CCH) + τ(CCC)	740.9 (0.37)	741.3 (0.30)
ϵ(CCH) + τ(CCC)	756.8 (0.22)	762.6 (0.60)
ϵ(CCH) + τ(CCC)	769.6 (1.00)	771.5 (1.00)
ϵ(CCH) + τ(CCC)	872.0 (0.64)	869.2 (0.96)
ϵ(CCH) + τ(CCC)	886.8 (0.05)	885.5 (0.06)
ϵ(CCH) + τ(CCC)	957.5 (0.15)	955.9 (0.33)
α(CCC) + β(CCH)	1022.1 (0.11)	1020.0 (0.07)
α(CCC) + β(CCH)	1026.0 (0.13)	1024.1 (0.06)
α(CCC) + β(CCH)	1094.7 (0.02)	1099.4 (0.01)
α(CCC) + β(CCH)	1114.3 (0.06)	1117.8 (0.05)
α(CCC) + β(CCH)	1145.6 (0.05)	1143.8 (0.05)
β(CCH) + *R*(CC)	1152.1 (0.08)	1150.6 (0.02)
β(CCH) + *R*(CC)	1174.2 (0.04)	1179.6 (0.02)
β(CCH) + *R*(CC)	1190.1 (0.15)	1191.3 (0.10)
β(CCH) + *R*(CC)	1225.3 (0.02)	1226.9 (0.05)
β(CCH) + *R*(CC)	1236.3 (0.02)	1233.1 (0.02)
β(CCH) + *R*(CC)	1258.3 (0.11)	1266.8 (0.11)
R(CC) + β(CCH)	1326.8 (0.20)	1315.5 (0.16)
β(CCH) + *R*(CC)	1341.4 (0.05)	1343.3 (0.12)
R(CC) + β(CCH)	1363.9 (0.02)	
ϵ(HC(sp^3)H) + *R*(CC)	1425.7 (0.31)	1414.7 (0.26)
β(CCH) + *R*(CC) + ϵ(HC(sp^3)H)	1439.0 (0.35)	1442.3 (0.22)
β(CCH) + *R*(CC)	1450.6 (0.06)	1447.6 (0.04)
β(CCH) + *R*(CC)	1471.6 (0.17)	1475.4 (0.17)
R(CC) + β(CCH)	1507.4 (0.25)	1507.5 (0.24)
R(CC)	1582.8 (0.02)	
R(CC)	1589.2 (0.03)	
R(CC)	1614.9 (0.03)	
R(CC)	1619.0 (0.03)	
R(CC)	1642.0 (0.06)	1645.2 (0.02) 1688−1945[f]
r(C(sp^3)H)	2961.7 (0.36)	2917.4 (0.15)
r(C(sp^3)H)	2985.6 (0.16)	2944.6 (0.10)
r(CH)	3094.2 (0.34)	3029.0 (0.44)[g]
r(CH)	3096.8 (0.03)	3032.0
r(CH)	3099.6 (0.02)	
r(CH)	3111.7 (0.96)	3065.7
r(CH)	3123.8 (1.27)	3071.0 (1.10)[h]

[a] Frequencies are given in cm^{-1}, and relative intensities are in parentheses. [b] Notation used: *R* and *r* are stretching modes, α and β are in-plane bending modes, and τ and ϵ are out-of-plane vibrations. [c] Harmonic-mode frequencies calculated at the B3LYP/6-311+G** level of theory (scaled by a factor of 0.98) based on the B3LYP/6-311G** optimized geometry. The integral intensity of the 769.6-cm^{-1} band is equal to 47 km/mol. [d] Only bands with relative intensities ≥0.02 are listed. [e] For each experimental band, only the most intense subband is listed. Relative intensities are scaled to the 771.5-cm^{-1} band as 1.0. The bands in the C−H stretching region are strongly overlapped; therefore, the assignments in this region are tentative. [f] Combination-band region containing bands at 1737.9 (0.01), 1752.9 (0.03), 1787.2 (0.01), 1810.0 (0.01), 1814.4 (0.02), 1898.5 (0.01), 1915.7 (0.01), 1940.3 (0.01), and 1944.7 cm^{-1} (0.03). [g] Relative intensity of the sum of the 3029.0- and 3032.0-cm^{-1} bands. [h] Relative intensity of the sum of the 3071.0- and 3065.7-cm^{-1} bands.

TABLE 2: Comparison of the Calculated (B3LYP / 6-311+G) and Experimental (Ar Matrix, 12 K) Infrared Absorption Spectrum of the 2,3-Benzofluorene Radical Cation[a]**

mode description[b]	calcd (B3LYP/6-311+G**)[c,d]	exptl (Ar matrix)[e]
α(CCC)	303.3 (0.02)	
τ(CCC)	439.1 (0.04)	
α(CCC)	617.2 (0.07)	
ϵ(CCH) + τ(CCC)	713.7 (0.09)	
α(CCC) + *R*(CC)	732.0 (0.16)	[f]
ϵ(CCH) + τ(CCC)	756.0 (0.05)	
ϵ(CCH) + τ(CCC)	780.9 (0.22)	[f]
ϵ(CCH) + τ(CCC)	891.9 (0.03)	
α(CCC) + β(CCH)	975.6 (0.04)	981.6 (0.04)
β(CCH) + *R*(CC)	1012.7 (0.05)	[g]
β(CCH) + *R*(CC)	1096.7 (0.07)	1099.3 (0.18)
β(CCH) + *R*(CC)	1137.4 (0.07)	1137.2 (0.32)
β(CCH) + *R*(CC)	1158.5 (0.39)	1151.1 (0.29)
β(CCH) + *R*(CC)	1175.4 (0.05)	1163.6 (0.04)
β(CCH) + *R*(CC)	1192.2 (0.03)	1180.8 (0.05)
β(CCH) + *R*(CC)	1203.0 (0.04)	
β(CCH) + *R*(CC)	1236.0 (0.42)	1241.5, 1245.3 (0.45)
β(CCH) + *R*(CC)	1280.4 (0.05)	1286.1 (0.04)
β(CCH) + *R*(CC)	1311.8 (0.55)	1305.5, 1309.6 (1.00)
β(CCH) + *R*(CC)	1340.1 (0.08)	1334.8, 1333.1 (0.11)
β(CCH) + *R*(CC)	1347.1 (0.46)	1357.8 (0.18)
β(CCH) + *R*(CC)	1359.2 (0.07)	1361.5 (0.03)
β(CCH) + *R*(CC) + ϵ(HC(sp^3)H)	1395.4 (0.09)	1387.7 (0.05)
β(CCH) + *R*(CC) + ϵ(HC(sp^3)H)	1417.7 (0.07)	1420.5 (0.04)
β(CCH) + *R*(CC)	1441.5 (0.28)	1447.1 (0.15)
β(CCH) + *R*(CC)	1456.6 (0.19)	1461.1 (0.18)
β(CCH) + *R*(CC)	1481.4 (0.10)	
R(CC)	1501.4 (0.05)	
R(CC)	1532.5 (0.06)	1537.7 (0.09)
R(CC)	1547.4 (0.35)	1553.0 (0.34)
R(CC)	1571.6 (1.00)	1567.2 (0.77)
R(CC)	1595.8 (0.26)	[h]
R(CC)	1598.0 (0.34)	[h]

[a] Frequencies are given in cm^{-1}, and relative intensities are in parentheses. [b] Notation used: *R* and *r* are stretching modes, α and β are in-plane bending modes, and τ and ϵ are out-of-plane vibrations. [c] Harmonic-mode frequencies calculated at the B3LYP/6-311+G** level of theory (scaled by a factor of 0.98) based on the B3LYP/6-311G** geometry. The integral intensity of the 1571.6-cm^{-1} band is equal to 417 km/mol. [d] Only bands with relative intensities ≥0.02 are listed. [e] For each experimental band, only the most intense subbands are listed. No cationic bands were observed in the C−H stretching region. The strongest calculated band (3142.0 cm^{-1}) in this region has a relative intensity of only 0.01. [f] This region is covered by the strong CCl_4 and CCl_3 bands. [g] Covered by the 1019.3-cm^{-1} CCl_3·Cl complex band. [h] Energy region covered by the H_2O bands.

the estimated ϵ_{IR} is thus 530 M^{-1} cm^{-1}. For the 869.2 cm^{-1} IR band, the measured absorbance is 0.01. For the 337.3 nm electronic band, the measured absorbance is 0.74. Thus, the estimated molar absorptivity, ϵ_{UV}, for the 337.3 nm band is 39 400 M^{-1} cm^{-1}.

The oscillator strength (*f*) for an electronic transition can be calculated from the molar absorptivities (ϵ) for each band associated with the particular transition:

$$f = 4.33 \times 10^{-9} \int \epsilon(\nu)\, d\nu \approx 4.33 \times 10^{-9} \sum \epsilon(\nu)\, \Delta\nu_{1/2} \quad (1)$$

Thus, after calculating the molar absorptivities for the observed 337.3 nm band (0−0) and its vibronic bands (Figure 6), the oscillator strength (*f*) for the $S_1 \leftarrow S_0$ transition of neutral BZF is estimated to be 0.024. *f* values for other electronic transitions of neutral and cationic BZF were determined similarly (cf. vide infra). Any error in the *f* values is mainly due to the accuracy of the calculated absolute integral intensity of the vibrational transitions as well as to the many vibrational progressions in the UV overlap (cf. Figure 6).

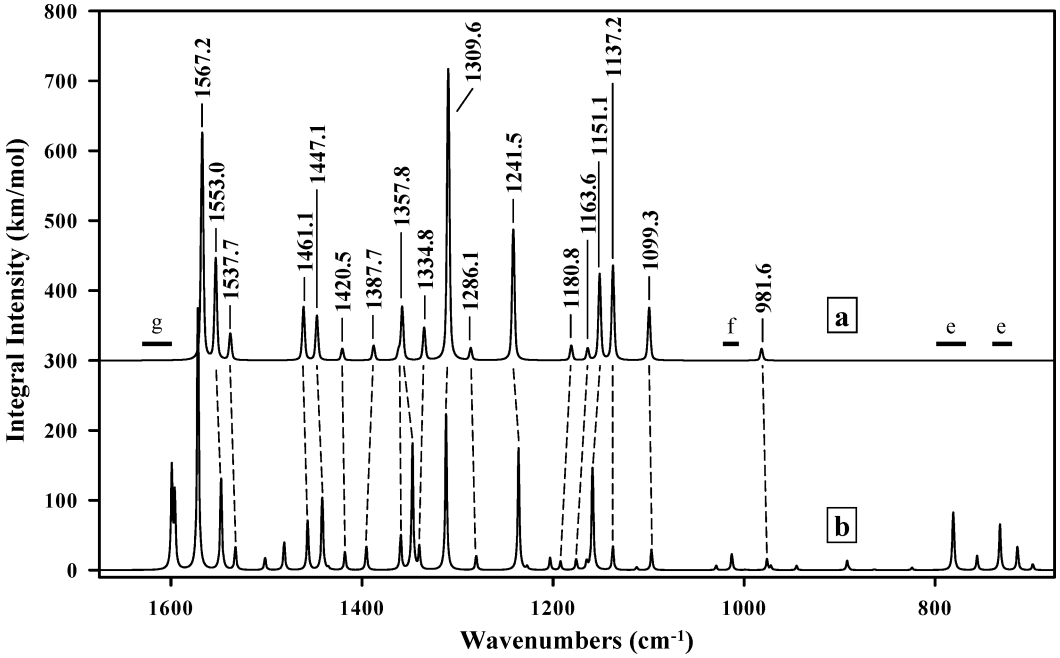

Figure 5. Synthetic experimental and calculated infrared absorption spectra (1675−675 cm^{-1}) for the 2,3-benzofluorene cation ($C_{17}H_{12}^{+}$). (a) Synthetic IR absorption spectrum of the 2,3-benzofluorene cation created from energies and relative intensities observed in solid Ar at 12 K. Inaccessible energy regions are marked by horizontal solid lines and described in similarly marked footnotes of Table 2. (b) IR absorption spectrum of the 2,3-benzofluorene cation calculated at the B3LYP/6-311+G** level of theory (scaled by 0.98).

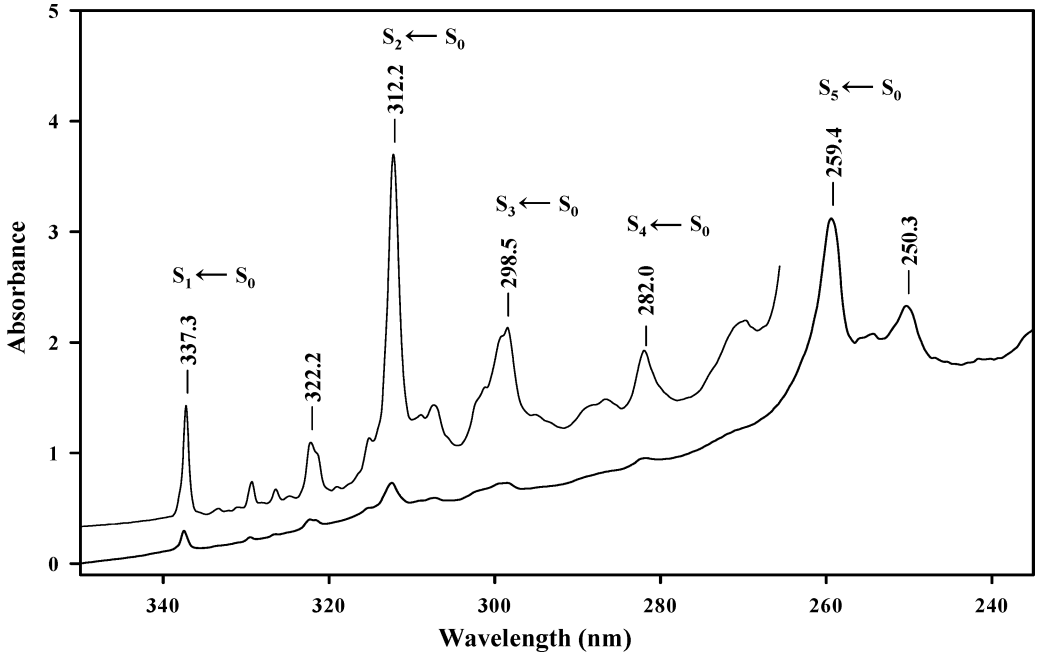

Figure 6. Electronic absorption spectrum (350−235 nm) of neutral 2,3-benzofluorene isolated in solid Ar at 12 K. Assigned transitions correspond to vertical excitation energies calculated at various levels of theory listed in Table 3.

2. BZF Cation. The UV−visible absorption spectrum, obtained after electron bombardment of the gas mixture, contains three new features at 714.5 nm (1.74 eV), 599.0 nm (2.07 eV), and 508.5 nm (2.44 eV) (cf. Figure 7). Annealing the matrix to 34 K decreases the 714.5 and 599.0 nm bands by 30 and 20%, respectively. The 508.5 nm band remains unchanged during annealing. Because of their reduction upon annealing, the 714.5 and 599.0 nm bands are assigned to cationic species. However, only the 714.5 nm band matches an electronic transition of the BZF cation (i.e., $D_3 \leftarrow D_0$, cf. Table 4). The 508.5 nm band is assigned to a neutral species because it is unaffected by matrix annealing.

Shida previously observed the 722 nm (1.72 eV) band (cf. Table 4) for the BZF cation in s-BuCl at 77 K.[41,42] The ca. 150 cm^{-1} blue shift in Ar is reasonable because for a smaller PAH cation (fluorene) a blue shift of ca. 490 cm^{-1} was observed previously.[29] The lowest-energy band observed for the BZF cation falls at ca. 1500 nm (0.8 eV),[41,42] which fits very well with the TDDFT-predicted energy of 0.77 eV ($D_1 \leftarrow D_0$ transition, cf. Table 4). On the basis of the TDDFT predictions, five experimental absorption bands, listed in Table 4, are assigned to separate electronic transitions, with a maximum error of 0.27 eV. The overall profile of the BZF cation absorption spectrum resembles that of fluorene.[29] A closer comparison

TABLE 3: Calculated and Observed Vertical Excitation Energies, ω, and Oscillator Strengths, f, for Neutral 2,3-Benzofluorene

	calcd[b] (BLYP)		calcd[c] (BLYP-AC)		calcd[d] (B3LYP-AC)		exptl	
state[a]	ω/eV	f	ω/eV	f	ω/eV	f	ω/eV	f[e]
$^1A'$ ($\pi_1 \leftarrow \pi_{-1}$)	3.53	0.124	3.53	0.122	3.91	0.201	3.68[e], 3.6[f]	0.024
			$^1A'$ ($\pi_1 \leftarrow \pi_{-1}$) + 1387 cm^{-1}				3.85[e], 3.8[f]	[g]
$^1A'$ ($\pi_1 \leftarrow \pi_{-2}$)	3.61	0.020	3.61	0.022	4.00	0.012	3.97[e], 3.9[f]	0.056
$^1A'$ ($\pi_3 \leftarrow \pi_{-1}$)	4.04	0.125	4.05	0.121	4.57	0.126	4.15[e], 4.1[f]	0.031
$^1A'$ ($\pi_1 \leftarrow \pi_{-3}$)	4.15	0.037	4.15	0.037	4.91	0.053	4.40[e], 4.3[f]	0.028
$^1A'$ ($\pi_2 \leftarrow \pi_{-1}$)	4.38	0.508	4.38	0.515	4.72	0.713	4.78[e], 4.7[f]	1.097
			$^1A'$ ($\pi_2 \leftarrow \pi_{-1}$) + 1401 cm^{-1}				4.95[e], 4.9[f]	[h]
$^1A'$ ($\pi_2 \leftarrow \pi_{-2}$)	4.46	0.047	4.46	0.043	5.08	0.035		
$^1A''$ ($\sigma_5 \leftarrow \pi_{-1}$)	4.52	0.002	4.59	0.002	5.23	0.001		
$^1A'$ ($\pi_1 \leftarrow \pi_{-4}$)	4.54	0.066	4.54	0.065	5.21	0.010		
$^1A''$ ($\sigma_6 \leftarrow \pi_{-1}$)	4.66	0.000	4.72	0.000	5.41	0.001		
$^1A'$ ($\pi_3 \leftarrow \pi_{-2}$)	4.69	0.091	4.69	0.089	5.32	0.080		
$^1A''$ ($\sigma_7 \leftarrow \pi_{-1}$)	4.73	0.000	4.80	0.000	5.45	0.000		
$^1A'$ ($\pi_8 \leftarrow \pi_{-1}$)	4.89	0.005	4.89	0.006	5.49	0.012		

[a] The ground-state wave function transforms as the A′ irreducible representation in C_s symmetry. The π and σ orbitals are numbered in order of increasing orbital energies. The π_{-1} and π_1 labels denote the highest doubly occupied and the lowest unoccupied π orbitals, respectively. The character of the transition given is based on the dominant excited determinant contribution in the BLYP TDDFT results. [b] Values calculated via TDDFT using the BLYP/6-31++G** functional/basis set at the B3LYP/6-31G** optimized geometry. [c] Values calculated via TDDFT using the BLYP/6-31++G** functional/basis set and the Casida−Salahub asymptotic correction with a shift of 1.996 eV at the B3LYP/6-31G** optimized geometry. [d] Values calculated via TDDFT using the B3LYP/6-31++G** functional/basis set and the Casida−Salahub asymptotic correction with a shift determined by the Zhan−Nichols−Dixon relationship at the B3LYP/6-31G** optimized geometry. [e] This work (solid Ar). Bands observed at 337.3, 322.2, 312.2, 298.5, 282.0, 259.4, and 250.3 nm, respectively. Tentative assignment for the $S_n \leftarrow S_0$ ($n \geq 4$) transitions is made. [f] NIST Chemistry Webbook (http://webbook.nist.gov/chemistry/). [g] This band is assigned to a vibronic band associated with the $S_1 \leftarrow S_0$ transition (see text). [h] This band is assigned to a vibronic band associated with the $S_5 \leftarrow S_0$ transition (see text).

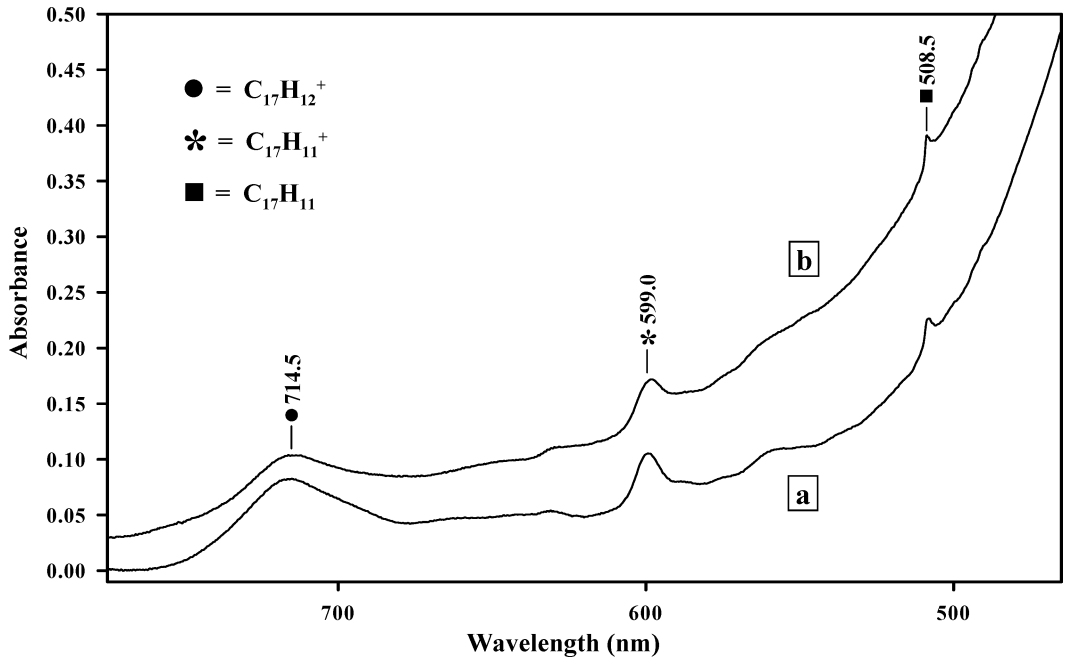

Figure 7. Electronic absorption spectra (775−465 nm) of neutral, cationic, and fragmented 2,3-benzofluorene isolated in solid Ar at 12 K. (a) Electronic absorption spectrum recorded after electron bombardment of an Ar/2,3-benzofluorene/CCl_4 (0.1%) gas mixture. (b) Electronic absorption spectrum recorded after annealing matrix a to 34 K.

reveals that the band positions are red shifted from their fluorene counterparts, undoubtedly a result of the greater delocalization in BZF. In our previous study, it was found that TDDFT reproduced subtle band-position shifts more accurately than might be expected from its absolute accuracy of only 0.3 eV.[28] In fact, the BLYP/6-31G** calculation predicts red shifts of approximately the right amounts for the $\pi_0 \leftarrow \pi_{-1}$, $\pi_0 \leftarrow \pi_{-3}$, and $\pi_1 \leftarrow \pi_0$ transitions on going from fluorene to BZF.

No additional bands were observed in the UV−visible or IR regions when CCl_4 was omitted from the Ar matrix gas. This implies that no significant concentration of BZF anions was formed in the current experiments. This is in line with the recently calculated (B3LYP/6-311G*) adiabatic electron affinity (EA) for the BZF of 0.26 eV (zero-point vibrational energy corrected, expected to be accurate to 0.2 eV).[43] In previous matrix experiments, negative ions were observed only for PAHs with estimated EAs of ca. 0.7 eV or larger.[28,44,45]

3. Singly Dehydrogenated BZF Neutral and Its Cation ($C_{17}H_{11}$ and $C_{17}H_{11}^+$). Because the 508.5 nm (2.44 eV) and 599.0 nm (2.07 eV) bands appeared only in electron bombardment experiments and were not assignable to neutral or cationic BZF, these bands are likely due to fragmentation products of BZF. Photolysis of the matrix with the full output of a 100-W medium-pressure Hg lamp for 5 h reduces the BZF cation's

TABLE 4: Calculated and Observed Vertical Excitation Energies, ω, and Oscillator Strengths, f, for the 2,3-Benzofluorene Radical Cation

	calcd[b] (BLYP/6-31G**)		exptl	
state[a]	ω/eV	f	ω/eV	f
$^2A''$ ($\pi_0 \leftarrow \pi_{-1}$)	0.77	0.013	~0.8[c]	
$^2A''$ ($\pi_0 \leftarrow \pi_{-2}$)	1.01	0.007		
$^2A''$ ($\pi_0 \leftarrow \pi_{-3}$)	1.87	0.119	1.72[d], 1.74[e]	0.034[e]
$^2A''$ ($\pi_0 \leftarrow \pi_{-4}$)	2.25	0.004		
$^2A''$ ($\pi_1 \leftarrow \pi_0$)	(2.87)	0.030	2.70[c]	
$^2A'$ ($\pi_0 \leftarrow \sigma_{-5}$)	2.89	0.000		
$^2A'$ ($\pi_0 \leftarrow \sigma_{-7}$)	3.00	0.000		
$^2A''$ ($\pi_1 \leftarrow \pi_{-1}$)	(3.13)	0.039	3.06[c]	
$^2A''$ ($\pi_0 \leftarrow \pi_{-6}$)	3.23	0.169	3.49[c]	
$^2A'$ ($\pi_0 \leftarrow \sigma_{-8}$)	3.34	0.000		
$^2A'$ ($\pi_0 \leftarrow \sigma_{-9}$)	3.39	0.000		
$^2A''$ ($\pi_1 \leftarrow \pi_{-2}$)	(3.47)	0.002		

[a] The ground-state wave function transforms as the A″ irreducible representation in C_s symmetry. The π and σ orbitals are numbered in order of increasing orbital energies. The π_{-1}, π_0, and π_1 labels denote the highest doubly occupied, highest singly occupied, and lowest unoccupied π orbitals, respectively. The character of the transition given is based on the dominant excited determinant contribution in the BLYP TDDFT results. [b] Values calculated via TDDFT using the BLYP/6-31G** functional/basis set at the B3LYP/6-31G** optimized geometry. The excitation energies in parentheses correspond to non-Koopmans' transitions when viewed as ionization from the neutral. [c] Reference 41. Transitions observed at 1500, 460, 430, 405, and 355 nm, respectively, in s-BuCl at 77 K. [d] Reference 42. Transition observed at 722 nm in the s-BuCl matrix at 77 K. [e] This work. Transition observed at 714.5 nm in solid Ar.

714.5 nm band by 47% (Figure 8) while at the same time increasing the 599.0 and 508.5 nm bands by 38 and 230%, respectively. A new band appearing at 490.8 nm can be attributed to a vibration built on the 508.5 nm 0−0 band. The 47% decrease of the 714.5 nm band results from the neutralization and fragmentation of the BZF cation. Because the 599.0 nm band has already been assigned to a cationic species of unknown structure, its 38% increase likely results from the fragmentation of the BZF cation. Because the 508.5 nm band was not reduced by matrix annealing, it is assigned to a neutral fragment of BZF.

The lowest calculated energy-fragmentation route for neutral (3.32 eV) and cationic (2.60 eV) BZF is the removal of a hydrogen atom (H_{11}) from the five-membered ring. Electron bombardment of gas-phase BZF prior to deposition or UV irradiation of trapped BZF neutrals and cations would likely yield singly dehydrogenated BZF neutrals ($C_{17}H_{11}$) and cations ($C_{17}H_{11}^+$) in the matrix. However, fragment bands were not observed after extensive photolysis (16 h) of isolated neutral BZF. Thus, the increase of the 508.5 nm band during UV irradiation must result from the neutralization of the BZF $C_{17}H_{11}^+$ fragment ion instead of the fragmentation of neutral BZF. The $C_{13}H_{10}^+ + h\nu \rightarrow C_{13}H_9 + H^+$ mechanism was originally suggested by Shida to explain the photoproduction of the fluorene neutral fragment from the fluorene cation radical,[41,42] but in the present context, this mechanism is not energetically favorable compared to cationic fragment neutralization.

Thus, the 599.0 and 508.5 nm bands are assigned to the cationic and neutral forms of the same BZF fragment, respectively. In similar fluorene ($C_{13}H_{10}$) experiments, hydrogen loss was observed after UV photolysis of trapped neutral and cationic fluorine[29] as well as from UV photolysis of an Ar matrix containing only neutral fluorene.[45] The energies required for the removal of the first hydrogen atom from the fluorene neutral and cation are 3.38 and 2.64 eV, respectively.[45] The 508.5 nm band is within 0.3 eV of the strongest transition ($D_3 \leftarrow D_0$) predicted by TDDFT calculations for $C_{17}H_{11}$ (Table 6). The calculated excitation energy is again insensitive to the asymptotic correction, which indicates that the excited-state wave function has a compact spatial profile. The observed 599.0 nm (2.07 eV) band is within 0.3 eV of the relatively strong $S_2 \leftarrow S_0$ transition predicted by TDDFT calculations for $C_{17}H_{11}^+$ (Table 5). Although the $S_9 \leftarrow S_0$ transition is predicted to be stronger than the $S_2 \leftarrow S_0$ transition, the strong BZF neutral bands at 312.2 or 298.5 nm most likely obscure the $S_9 \leftarrow S_0$ band of $C_{17}H_{11}^+$. Because $C_{17}H_{11}$ and $C_{17}H_{11}^+$ were not observed in the IR absorption spectrum, experimental oscillator strengths could not be determined for the 599.0 and 508.5 nm bands.

The predicted integral IR intensities for $C_{17}H_{12}^+$ are much larger than for the $C_{17}H_{11}$ neutral (417 km/mol vs 70 km/mol), and their respective electronic bands at 714.7 and 508.5 nm have different band shapes and predicted oscillator strengths, f. The fwhm of the ion's 714.7 nm band is 4 times broader (in cm^{-1}) (cf. Figure 7) and has half the calculated f value of the neutral's 508.5 nm band. Therefore, the deduced concentration ratio of $C_{17}H_{12}^+$ to $C_{17}H_{11}$ from spectrum a of Figure 7 (where the absorbance ratio of $C_{17}H_{12}^+$ to $C_{17}H_{11}$ is ca. 3.5) is 28. Thus, the strongest IR absorbance of matrix-isolated $C_{17}H_{11}$ in Figure 7 is estimated to be ca. $417/70 \times 28 \approx 167$ times lower than the strongest $C_{17}H_{12}^+$ IR absorbance (0.015). Furthermore, this is below the observable limit of 8×10^{-4}. A similar procedure, applied to the $C_{17}H_{12}^+$ fragment ion, yielded an estimate of the experimentally predicted strongest IR band absorbance of 7×10^{-4} at 1367 cm^{-1}. The strongest calculated IR band at 1600 cm^{-1} (593 km/mol) (2.7 times stronger than at 1367 cm^{-1}) is expected to be overlapped by water bands and was therefore impossible to extract from the experimental spectrum.

V. Comparison to UIR Emission Features

Several infrared absorption bands observed for the BZF cation match the UIR emission features. The strong bands at 1305.5 cm^{-1} (7.66 μm) and 1309.6 cm^{-1} (7.64 μm) correlate well with the most intense UIR band at 7.7 μm. The 1245.3 cm^{-1} (8.03 μm), 1241.5 cm^{-1} (8.05 μm), 1151.1 cm^{-1} (8.69 μm), and 1137.2 cm^{-1} (8.79 μm) bands fit within the broad UIR envelope defined by the 7.7 and 8.6 μm features. The band at 1567.2 cm^{-1} (6.38 μm) is close to the 6.2 μm emission feature. Potential bands contributing to the 11.3 μm (885 cm^{-1}) UIR feature may be obscured by the strong CCl_3 band at 897.9 cm^{-1} or the BZF neutral band at 869.2 cm^{-1}. The calculated IR absorption spectrum for the BZF cation contains bands in this obscured experimental range. The predicted weak band at 891.9 cm^{-1} (11.2 μm) may contribute to the 11.3 μm feature. Thus, IR absorption bands for the BZF cation may account for the 6.2, 7.7, 8.6, and 11.3 μm UIR emission features. However, no bands were observed in the 3000 cm^{-1} (3.3 μm) region of the BZF cation spectrum.

The relative band intensities in the infrared absorption spectrum of the BZF cation also correlate well with the UIR emission spectrum. For the BZF cation, the C−C stretching and C−H in-plane bending modes in the 1100−1650 cm^{-1} (9.1−6.1 μm) range are more intense than the C−H out-of-plane bending modes in the 700−1000 cm^{-1} (14.3−10.0 μm) range. The 1305.5 cm^{-1} (7.66 μm), 1309.6 cm^{-1} (7.64 μm), and 1567.2 cm^{-1} (6.38 μm) bands are the strongest bands observed in the experimental spectrum. They are at least 20 times more intense than the experimental 981.6 cm^{-1} (10.2 μm) band. Thus, the observed intensity pattern for the BZF cation correlates well

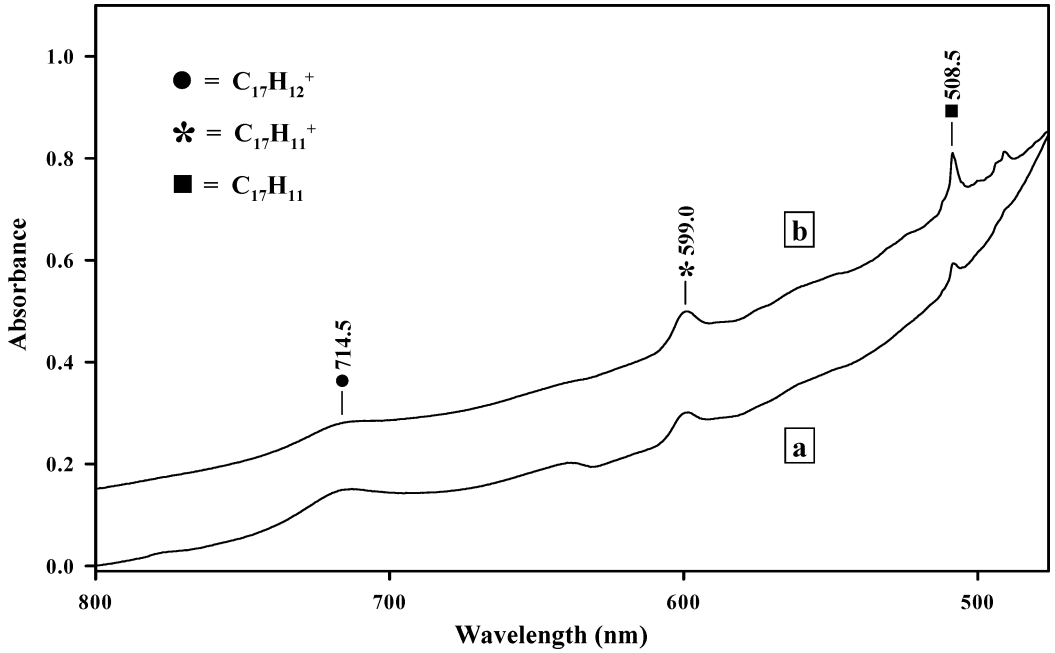

Figure 8. Electronic absorption spectra (800−475 nm) of neutral, cationic, and fragmented 2,3-benzofluorene isolated in solid Ar at 12 K. (a) Electronic absorption spectrum recorded after electron bombardment of an Ar/2,3-benzofluorene/CCl_4 (0.1%) gas mixture. (b) Electronic absorption spectrum recorded after irradiating matrix a with the output of a 100-W medium-pressure Hg lamp for 5 h.

TABLE 5: Calculated and Observed Vertical Excitation Energies, ω, and Oscillator Strengths, f, for the 2,3-Benzofluorene-like $C_{17}H_{11}$ Cation[a]

	calcd[c] (BLYP/6-31G**)		exptl[d]	
state[b]	ω/eV	f	ω/eV	f
$^1A'$ ($\pi_1 \leftarrow \pi_{-1}$)	1.32	0.002		
$^1A'$ ($\pi_1 \leftarrow \pi_{-2}$)	2.26	0.249	2.07	
$^1A'$ ($\pi_1 \leftarrow \pi_{-3}$)	2.62	0.013		
$^1A'$ ($\pi_1 \leftarrow \pi_{-4}$)	3.37	0.039		
$^1A'$ ($\pi_1 \leftarrow \pi_{-5}$)	3.54	0.025		
$^1A''$ ($\pi_1 \leftarrow \sigma_{-6}$)	3.74	0.000		
$^1A'$ ($\pi_2 \leftarrow \pi_{-2}$)	(3.89)	0.011		
$^1A''$ ($\pi_1 \leftarrow \sigma_{-7}$)	3.91	0.000		
$^1A'$ ($\pi_2 \leftarrow \pi_{-1}$)	(4.16)	0.946		
$^1A''$ ($\pi_1 \leftarrow \sigma_{-9}$)	4.22	0.000		
$^1A''$ ($\pi_1 \leftarrow \sigma_{-10}$)	4.29	0.000		

[a] Compare with Figure 1b. [b] The ground-state wave function transforms as the A′ irreducible representation in C_s symmetry. The π and σ orbitals are numbered in order of increasing orbital energies. The π_{-1} and π_1 labels denote the highest doubly occupied and the lowest unoccupied π orbitals, respectively. The character of the transition given is based on the dominant excited determinant contribution in the BLYP TDDFT results. [c] Values calculated via TDDFT using the BLYP/6-31G** functional/basis set at the B3LYP/6-31G** optimized geometry. [d] This work. Transition observed at 599.0 nm in solid Ar. No f value was established because no IR band was observed.

TABLE 6: Calculated and Observed Vertical Excitation Energies, ω, and Oscillator Strengths, f, of the 2,3-Benzofluorene-like $C_{17}H_{11}$ Neutral Radical[a]

	calcd[c] (BLYP/6-31++G**)		calcd[d] (BLYP-AC/6-31++G**)		exptl[e]	
state[b]	ω/eV	f	ω/eV	f	ω/eV	f
$^2A''$ ($\pi_0 \leftarrow \pi_{-1}$)	1.65	0.004	1.65	0.004		
$^2A''$ ($\pi_1 \leftarrow \pi_0$)	2.00	0.016	2.00	0.015		
$^2A''$ ($\pi_0 \leftarrow \pi_{-2}$)	2.21	0.059	2.21	0.059	2.44	
$^2A''$ ($\pi_1 \leftarrow \pi_{-1}$)	2.81	0.002	2.81	0.002		
$^2A''$ ($\pi_0 \leftarrow \pi_{-3}$)	2.88	0.000	2.88	0.000		
$^2A''$ ($\pi_2 \leftarrow \pi_0$)	3.10	0.040	3.10	0.040		
$^2A''$ ($\pi_0 \leftarrow \pi_{-4}$)	3.21	0.009	3.21	0.009		
$^2A''$ ($\pi_1 \leftarrow \pi_{-2}$)	3.35	0.002	3.35	0.002		
$^2A''$ ($\pi_3 \leftarrow \pi_0$)	3.48	0.001	3.48	0.001		
$^2A''$ ($\pi_0 \leftarrow \pi_{-5}$)	3.60	0.024	3.59	0.023		
$^2A'$ ($\sigma_4 \leftarrow \pi_0$)	3.69	0.000	3.76	0.000		

[a] Compare with Figure 1b. [b] The ground-state wave function transforms as the A″ irreducible representation in C_s symmetry. The π and σ orbitals are numbered in order of increasing orbital energies. The π_{-1}, π_0, and π_1 labels denote the highest doubly occupied, highest singly occupied, and lowest unoccupied π orbitals, respectively. The character of the transition given is based on the dominant excited determinant contribution in the BLYP TDDFT results. [c] Values calculated via TDDFT using the BLYP/6-31++G** functional/basis set at the B3LYP/6-31G** optimized geometry. [d] Values calculated via TDDFT using the BLYP/6-31++G** functional/basis set and the Casida−Salahub asymptotic correction with the shift of 1.988 eV at the B3LYP/6-31G** optimized geometry. [e] This work. Transition observed at 508.5 nm in solid Ar. No f value was established because no IR band was observed.

with the relative intensities of the UIR emission spectrum, in which the 6.2, 7.7, and 8.6 μm features are observed to be stronger than the 11.3 μm feature.

Because of its low concentration, the singly dehydrogenated BZF fragment ion ($C_{17}H_{11}^+$) was not observed in the IR spectrum. However, strongest bands are predicted at 1600.0 cm^{-1} (6.25 μm), 1366.6 cm^{-1} (7.32 μm), and 1121.0 cm^{-1} (8.92 μm). The 7.32 μm and 8.92 μm bands do not correlate well with the UIR emission features at 7.7 μm and 8.6 μm. Furthermore, the calculated 767.1 cm^{-1} (13.0 μm) band does not appear in the UIR emission spectrum. Thus, the $C_{17}H_{11}^+$ fragment ion does not appear to be a significant contributor to the UIR emission features.

VI. Conclusions

In this study, infrared vibrational and UV−visible electronic absorption spectra of 2,3-benzofluorene and its cation trapped in solid Ar were recorded. Band assignments have been made on the basis of predicted (B3LYP/6-311+G** at B3LYP/6-311G** optimized geometry) harmonic-mode vibrational frequencies and TDDFT (BLYP/6-31++G**, B3LYP/6-31++G** with Casida−Salahub asymptotic correction and the B3LYP/6-31G** optimized geometry) vertical electronic

excitation energies and oscillator strengths. The observed mid-IR absorption spectra are described quite well by theory with all bands assignable with an average (maximum) position error of 3.1 (11.3) cm^{-1} for the BZF neutral and 5.8 (11.8) cm^{-1} for the BZF cation. The observed electronic bands of the singly dehydrogenated BZF neutral and cation are assigned on the basis of TDDFT (BLYP/6-31G**) predictions. Experimental evidence shows that the production of the former fragment must result from the neutralization of the BZF fragment cation instead of the photofragmentation of neutral BZF.

BZF and its cation possess infrared bands that match well with the unidentified infrared emission bands from interstellar space, but their photofragments do not.

Acknowledgment. We gratefully acknowledge the National Aeronautics and Space Administration and the donors of the Petroleum Research Fund, administered by the American Chemical Society, for their support of this research. S.H.'s research was performed in part using the Molecular Science Facility (MSCF) in the William R. Wiley Environmental Molecular Sciences Laboratory at the Pacific Northwest National Laboratory (PNNL). The MSCF is funded by the Office of Biological and Environmental Research in the U.S. Department of Energy. PNNL is operated by Battelle for the U.S. Department of Energy under contract DE-AC06-76RLO 1830. J.S. and M.V. thank Dr. Tadamasa Shida (Kanagawa Institute of Technology, Japan) for helpful discussions.

References and Notes

(1) Gillett, F. C.; Forrest, W. J.; Merrill, K. M. *Astrophys. J.* **1973**, *183*, 87.

(2) Duley, W. W.; Williams, D. A. *Mon. Not. R. Astron. Soc.* **1981**, *196*, 269.

(3) Leger, A.; Puget, J. L. *Astron. Astrophys.* **1984**, *137*, L5.

(4) Allamandola, L. J.; Tielens, A. G. G. M.; Barker, J. R. *Astrophys. J.* **1985**, *290*, L25.

(5) Szczepanski, J.; Vala, M. *Astrophys. J.* **1993**, *414*, 646.

(6) Szczepanski, J.; Vala, M. *Nature* **1993**, *363*, 699.

(7) Hudgins, D. M.; Sandford, S. A.; Allamandola, L. J. *J. Phys. Chem.* **1994**, *98*, 4243.

(8) Hudgins, D. M.; Allamandola, L. J. *J. Phys. Chem.* **1995**, *99*, 3033.

(9) Geballe, T. R.; Tielens, A. G. G. M.; Allamandola, L. J.; Moorhouse, A.; Brand, P. W. J. L. *Astrophys. J.* **1989**, *341*, 278.

(10) Geballe, T. R.; Lacy, J. H.; Persson, S. E.; McGregor, P. J.; Soifer, B. T. *Astrophys. J.* **1985**, *292*, 500.

(11) Nagata, T.; Tokunaga, A. T.; Sellgren, K.; Smith, R. G.; Onaka, T.; Nakada, Y.; Sakata, A. *Astrophys. J.* **1988**, *326*, 157.

(12) Joblin, C.; Tielens, A. G. G. M.; Geballe, T. R.; Wooden, D. H. *Astrophys. J.* **1996**, *460*, L119.

(13) Oomens, J.; van Roij, A. J. A.; Meijer, G.; von Helden, G. *Astrophys. J.* **2000**, *542*, 404.

(14) Piest, J. A.; Oomens, J.; Bakker, J.; von Helden, G.; Meijer, G. *Spectrochim. Acta, Part A* **2001**, *57*, 717.

(15) Oomens, J.; Meijer, G.; von Helden, G. *J. Phys. Chem. A* **2001**, *105*, 8302.

(16) Schlemmer, S.; Cook, D. J.; Harrison, J. A.; Wurfel, B.; Chapman, W.; Saykally, R. J. *Science* **1994**, *265*, 1686.

(17) Cook, D. J.; Schlemmer, S.; Balucani, N.; Wagner, D. R.; Steiner, B.; Saykally, R. J. *Nature* **1996**, *380*, 227.

(18) Kim, H. S.; Wagner, D, R.; Saykally, R. J. *Phys. Rev. Lett.* **2001**, *86*, 5691.

(19) Pauzat, F.; Talbi, D.; Ellinger, Y. *Astron. Astrophys.* **1997**, *319*, 318.

(20) Boissel, P.; Lefevre, G.; Thiebot, P. *Molecules and Grains in Space*; Nenner, I., Ed; American Institute of Physics Press: New York, 1993; p 667.

(21) Boissel, P.; de Parseval, P.; Marty, P.; Lefevre, G. *J. Chem. Phys.* **1997**, *106*, 4973.

(22) Ekern, S. P.; Marshall, A. G.; Szczepanski, J.; Vala, M. *Astrophys. J.* **1997**, *488*, L39.

(23) Ekern, S. P.; Marshall, A. G.; Szczepanski, J.; Vala, M. *J. Phys. Chem. A* **1998**, *102*, 3498.

(24) Dibben, M. J.; Kage, D.; Szczepanski, J.; Eyler, J. R.; Vala, M. *J. Phys. Chem.* **2001**, *105*, 6024.

(25) Frisch, M. J.; Trucks, G. W.; Schlegel, H. B.; Scuseria, G. E.; Robb, M. A.; Cheeseman, J. R.; Zakrzewski, V. G.; Montgomery, J. A., Jr.; Stratmann, R. E.; Burant, J. C.; Dapprich, S.; Millam, J. M.; Daniels, A. D.; Kudin, K. N.; Strain, M. C.; Farkas, O.; Tomasi, J.; Barone, V.; Cossi, M.; Cammi, R.; Mennucci, B.; Pomelli, C.; Adamo, C.; Clifford, S.; Ochterski, J.; Petersson, G. A.; Ayala, P. Y.; Cui, Q.; Morokuma, K.; Malick, D. K.; Rabuck, A. D.; Raghavachari, K.; Foresman, J. B.; Cioslowski, J.; Ortiz, J. V.; Stefanov, B. B.; Liu, G.; Liashenko, A.; Piskorz, P.; Komaromi, I.; Gomperts, R.; Martin, R. L.; Fox, D. J.; Keith, T.; Al-Laham, M. A.; Peng, C. Y.; Nanayakkara, A.; Gonzalez, C.; Challacombe, M.; Gill, P. M. W.; Johnson, B. G.; Chen, W.; Wong, M. W.; Andres, J. L.; Head-Gordon, M.; Replogle, E. S.; Pople, J. A. *Gaussian 98*, revision A.3; Gaussian, Inc.: Pittsburgh, PA, 1998.

(26) Bauschlicher, C. W. *Astrophys. J.* **1998**, *509*, L125.

(27) Langhoff, S. R. *J. Phys. Chem.* **1996**, *100*, 2819.

(28) Hirata, S.; Head-Gordon, M.; Szczepanski, J.; Vala, M. *J. Phys. Chem. A* **2003**, *107*, 4940 and references therein.

(29) Szczepanski, J.; Banisaukas, J.; Vala, M.; Hirata, S.; Bartlett, R. J.; Head-Gordon, M. *J. Phys. Chem. A* **2002**, *106*, 63.

(30) Casida, M. E.; Jamorski, C.; Casida, K. C.; Salahub, D. R. *J. Chem. Phys.* **1998**, *108*, 4439.

(31) Tozer, D. J.; Handy, N. C. *J. Chem. Phys.* **1998**, *109*, 10180.

(32) Casida, M. E.; Salahub, D. R. *J. Chem. Phys.* **2000**, *113*, 8918.

(33) Hirata, S.; Zhan, C.-G.; Aprà, E.; Windus, T.; Dixon, D. A. *J. Phys. Chem. A* **2003**, *107*, 10154.

(34) *NWChem: A Computational Chemistry Package for Parallel Computers, A Development Version*; Pacific Northwest National Laboratory: Richland, WA, 2003.

(35) Szczepanski, J.; Vala, M.; Talbi, D.; Parisel, O.; Ellinger, Y. *J. Chem. Phys.* **1993**, *98*, 4494.

(36) Banisaukas, J.; Szczepanski, J.; Eyler, J.; Vala, M.; Hirata, S.; Head-Gordon, M.; Oomens, J.; Meijer, G.; von Helden, G. *J. Phys. Chem. A* **2003**, *107*, 782.

(37) Szczepanski, J.; Roser, D.; Personette, W.; Eyring, M.; Pellow, R.; Vala, M. *J. Phys. Chem.* **1992**, *96*, 7876 and references therein.

(38) Huneycutt, A. J.; Casaes, R. N.; McCall, B. J.; Chung, C. Y.; Lee, Y. P.; Saykally, R. J. http://dib.berkeley.edu/~bjmccall/preprints/PAH.pdf.

(39) Hudgins, D. M.; Bauschlicher, C. W., Jr.; Allamandola, L. J.; Fetzer, J. C. *J. Phys. Chem. A* **2000**, *104*, 3655.

(40) Bauschlicher, C. W., Jr.; Hudgins, D. M.; Allamandola, L. J. *Theor. Chem. Acc.* **1999**, *103*, 154.

(41) Shida, T. *Electronic Absorption Spectra of Radical Ions*; Elsevier: Amsterdam, 1988.

(42) Shida, T. Private communication, 2003.

(43) Gonzales, J. M.; Barden, C. J.; Brown, S. T.; von Raque Schleyer, P.; Schaefer, H. F., III; Li, Q. S. *J. Am. Chem. Soc.* **2003**, *125*, 1064.

(44) Moustfaoui, T.; Rebrion-Rowe, C.; Le Garrec, J.; Rowe, B. R.; Mitchell, J. B. A. *Faraday Discuss.* **1998**, *109*, 71.

(45) Halasinski, T. M.; Weisman, J. L.; Ruiterkamp, R.; Lee, T. J.; Salama, F.; Head-Gordon, M. *J. Phys. Chem. A* **2003**, *107*, 3660.

(46) Szczepanski, J.; Banisaukas, J.; Vala, M.; Hirata, S.; Wiley, W. R. *J. Phys. Chem. A* **2002**, *106*, 6935.

(47) Banisaukas, J.; Szczepanski, J.; Eyler, J.; Vala, M. *J. Phys. Chem. A* **2004**, *108*, 3723.